

High-pressure elastic anisotropy and superconductivity of hafnium:A first-principles calculation

Cheng-Bin Zhang(张成斌), Wei-Dong Li(李卫东), Ping Zhang(张平), Bao-Tian Wang(王保田)
Citation: Chin. Phys. B, 2021, 30 (**5**): 056202. DOI: 10.1088/1674-1056/abd6f6
Journal homepage: http://cpb.iphy.ac.cn; http://iopscience.iop.org/cpb

What follows is a list of articles you may be interested in

Structural, mechanical, electronic properties, and Debye temperature of quaternary carbide Ti_3NiAl_2C ceramics under high pressure: A first-principles study

Diyou Jiang(姜迪友), Wenbo Xiao(肖文波), and Sanqiu Liu(刘三秋)
Chin. Phys. B, 2021, 30 (**3**): 036202. DOI: 10.1088/1674-1056/abca20

Structural, mechanical, and electronic properties of Zr-Te compounds from first-principles calculations

Peng Wang(王鹏), Ning-Chao Zhang(张宁超), Cheng-Lu Jiang(蒋城露), Fu-Sheng Liu(刘福生), Zheng-Tang Liu(刘正堂), Qi-Jun Liu(刘其军)
Chin. Phys. B, 2020, 29 (**7**): 076201. DOI: 10.1088/1674-1056/ab8da7

Electronic structure and phase transition engineering in NbS_2: Crucial role of van der Waals interactions

Wei Wang(王威), Wen Lei(雷文), Xiaojun Zheng(郑晓军), Huan Li(黎欢), Xin Tang(唐鑫), Xing Ming(明星)
Chin. Phys. B, 2020, 29 (**5**): 056201. DOI: 10.1088/1674-1056/ab8214

First-principles investigation on ideal strength of B2 NiAl and NiTi alloys

Chun-Yao Zhang(张春尧), Fu-Yang Tian(田付阳), Xiao-Dong Ni(倪晓东)
Chin. Phys. B, 2020, 29 (**3**): 036201. DOI: 10.1088/1674-1056/ab7440

Surperhard monoclinic BC_6N allotropes: First-principles investigations

Nian-Rui Qu(屈年瑞), Hong-Chao Wang(王洪超), Qing Li(李青), Yi-Ding Li(李一鼎), Zhi-Ping Li(李志平), Hui-Yang Gou(缑慧阳), Fa-Ming Gao(高发明)
Chin. Phys. B, 2019, 28 (**9**): 096201. DOI: 10.1088/1674-1056/ab3439

High-pressure elastic anisotropy and superconductivity of hafnium: A first-principles calculation*

Cheng-Bin Zhang(张成斌)[1,2,3], Wei-Dong Li(李卫东)[1], Ping Zhang(张平)[4], and Bao-Tian Wang(王保田)[2,3,4,†]

[1] *Institute of Theoretical Physics and Department of Physics, and Collaborative Innovation Center of Extreme Optics, Shanxi University, Taiyuan* 030006, *China*

[2] *Institute of High Energy Physics, Chinese Academy of Sciences, Beijing* 100049, *China*

[3] *Spallation Neutron Source Science Center, Dongguan* 523803, *China*

[4] *LCP, Institute of Applied Physics and Computational Mathematics, Beijing* 100088, *China*

(Received 27 July 2020; revised manuscript received 18 December 2020; accepted manuscript online 28 December 2020)

The elastic anisotropy and superconductivity upon hydrostatic compression of α, ω, and β Hf are investigated using first-principle methods. The results of elastic anisotropies show that they increase with increasing pressure for α and ω phases, while decrease upon compression for β phase. The calculated superconducting transition temperatures are in excellent agreement with experiments. Electron–phonon coupling constants (λ) are increasing with pressure for α and ω phases, while decreasing for β phase. For β phase, the large values of λ are mainly due to the obvious TA1 soft mode. Under further compression, the TA1 soft vibrational mode will disappear gradually.

Keywords: first-principles, elastic anisotropy, superconductivity, hafnium

PACS: 62.20.–x, 62.20.de, 63.20.–e, 74.70.–b **DOI:** 10.1088/1674-1056/abd6f6

1. Introduction

Hafnium and its alloys have a narrow d-band. For these d-band materials, the d-electron orbital occupation and pressure-induced s–d electron transfer are crucial for the structural stability, electronic transitions, and superconducting properties.[1–6] Till now, phase transformation and mechanical properties of Hf have been reported in experiments[7–11] and calculations[2–4,11–15] widely. Also, the experimental results of superconducting transition temperature (T_c) upon crystallographic phases under pressure for Hf have been reported by Brshkin *et al.*[16] However, the theoretical investigations of its superconductivity are not sufficient.

Under ambient conditions, Hf metal crystallizes in a hexagonal close packed (hcp) structure (α phase).[9,17,18] Upon compressing, the α phase transforms into a so-called ω phase (hexagonal, space group $P6/mmm$).[9,11,18] Under further compression, the ω phase transforms into a body centered cubic (bcc) phase (β phase).[9,10] In previous theoretical and experimental reports, the transition pressures of $\alpha \rightarrow \omega$ ($\omega \rightarrow \beta$) are in range of 13.9–50 (30.7–73.1) GPa.[3,9–11,14,15,18] Structure changes will inevitably lead to performance changes. For example, the experimental results have confirmed that Hf metal exhibits the superconducting properties,[7,16,19–21] and the values of T_c are directly associated with their pressure-induced phase transitions. Under normal conditions, for α phase, the value of T_c is 0.128 K.[7,19,20] The effects of pressure on T_c are positive for α and ω phases, which results in an increase of T_c under compression.[16,21–23] The values of T_c are increasing until the ω phase transforms to the β phase.[16] This high-pressure superconductivity behavior has not been theoretically studied in literature.

In our previous studies, the pressure-dependent behaviors, such as phase transition, elastic constants, elastic moduli, phonon spectra, and thermodynamic properties, have been systematically investigated for Hf.[3] In the present work, we would like to extend our study to investigate these behaviors of elastic anisotropy and superconductivity under pressure.

2. Computational methods

2.1. Computational details

The pseudopotential plane-wave method[24] is used to calculate the electronic properties, lattice dynamics, and electron–phonon coupling (EPC) within the Perdew–Burke–Ernzerhof(PBE) generalized gradient approximation (GGA)[25] through the QUANTUM-ESPRESSO (QE) package.[26] The $5s^2 5p^6 5d^2 6s^2$ electrons are treated as valence electrons. A kinetic energy cutoff of 100 Ry is used for all three phases, as well as Gaussians width of 0.02 Ry. The k-point meshes of $24\times24\times16$, $16\times16\times24$, and $32\times32\times32$ are employed for α, ω, and β phases, respectively. The phonon spectra and phonon density of states (PhDOS) are computed using the density-functional perturbation theory (DFPT)[27]

*Project supported by the National Natural Science Foundation of China (Grant Nos. 11874247 and U1530258), the National Key R&D Program of China (Grant No. 2017YFA0304500), the 111 Plan of China (Grant No. D18001), the Hundred Talent Program of the Shanxi Province (2018), and the Program of State Key Laboratory of Quantum Optics and Quantum Optics Devices of China (Grant Nos. KF201703 and KF201904).

†Corresponding author. E-mail: wangbt@ihep.ac.cn

© 2021 Chinese Physical Society and IOP Publishing Ltd

with 6×6×4, 4×4×6, and 8×8×8 q-point meshes for α, ω, and β phases, respectively.

2.2. Superconductivity

The superconducting transition temperature T_c can be obtained from the Allen–Dynes modified McMillan equation[28,29]

$$T_c = \frac{\omega_{\log}}{1.2} \exp\left[-\frac{1.04(1+\lambda)}{\lambda-\mu^*(1+0.62\lambda)}\right], \quad (1)$$

where the $\omega_{\log}$ is the logarithmic average frequency, which can be written as

$$\omega_{\log} = \exp\left[\frac{2}{\lambda}\int_0^{\infty}\frac{\mathrm{d}\omega}{\omega}\alpha^2F(\omega)\ln\omega\right]; \quad (2)$$

λ and μ^* are the electron–phonon coupling constant and the Coulomb pseudopotential, respectively, with

$$\lambda = \int_0^{\infty}\frac{\alpha^2F(\omega)}{\omega}\mathrm{d}\omega. \quad (3)$$

The $\alpha^2F(\omega)$, Eliashberg electron–phonon spectral function, is written as

$$\alpha^2F(\omega) = \frac{1}{2\pi N(E_F)}\sum_{q\nu}\frac{\gamma_{q\nu}}{\omega_{q\nu}}\delta(\omega-\omega_{q\nu}), \quad (4)$$

where $N(E_F)$ is the electronic density of state (DOS) at the Fermi level, $\gamma_{q\nu}$ is the phonon linewidth, $\omega_{q\nu}$ is the phonon frequency. The $\gamma_{q\nu}$ is calculated by

$$\gamma_{q\nu} = \frac{2\pi\omega_{q\nu}}{\Omega_{BZ}}\sum_{n,k,m}|\,g^{\nu}_{kn,k+qm}\,|^2\,\delta(\varepsilon_{kn}-\varepsilon_F)\delta(\varepsilon_{k+qm}-\varepsilon_F), \quad (5)$$

where Ω_{BZ} is the volume of Brillouin zone (BZ), ε_{kn} and ε_{k+qm} represent the Kohn–Sham energy, and $g^{\nu}_{kn,k+qm}$ is the EPC matrix element. The $g^{\nu}_{kn,k+qm}$, determined self-consistently by the linear response theory, describes the probability amplitude for the scattering of an electron with a transfer of crystal momentum q.[28]

3. Results and discussion

3.1. Anisotropy of elastic moduli

In our previous investigation,[3] Hf metal crystallizes in α phase under ambient conditions. The transition pressure of $\alpha \to \omega$ ($\omega \to \beta$) is 44.8 (73.1) GPa, which is in good agreement with the experimental result of 38±8 (72±1) GPa reported by Xia *et al.*[9] The crystal structures for α, ω, and β phases are shown in Figs. 1(a)–1(c), as well as the indices of crystal direction and plane for hexagonal and cubic structures in Figs. 1(d) and 1(e). The pressure-dependent behaviors of the elastic constants and elastic moduli for Hf element have been systematically reported, as well as the detailed data of elastic constants, which can be found in Ref. [3]. Based on the calculated elastic constants, we extend our study to investigate the behavior of elastic anisotropy. Many low symmetry crystals exhibit a high degree of elastic anisotropy, which is closely related to the possibility of inducing micro-cracks in materials. The elastic anisotropy can be described by the universal anisotropic index A^U[30] and the percent anisotropy in compression and shear (A_{comp} and A_{shear}).[31,32] A^U, A_{comp}, and A_{shear} for a crystal are given as follows:

$$A^U = 5\frac{G_V}{G_R} + \frac{B_V}{B_R} - 6 \geq 0, \quad (6)$$

$$A_{comp} = \frac{B_V - B_R}{B_V + B_R}, \quad A_{shear} = \frac{G_V - G_R}{G_V + G_R}, \quad (7)$$

where B_V (G_V) and B_R (G_R) are the bulk modulus (shear modulus) in the Voigt–Reuss–Hill (VRH) approximations,[33–35] respectively. Please see the detailed computation scheme of the B_V, B_R, G_V, and G_R in Ref. [6] for the hexagonal crystal and in Ref. [37] for cubic structure. When a solid is isotropic, $A^U = 0$. The large deviation of A^U from 0 indicates the large extent of single crystal anisotropy. Thus, A^U represents a universal measure to quantify the elastic anisotropy.[30] The values of A_{comp} and A_{shear} can range from 0 to 1, where 0 (1) represents the isotropic (the maximum elastic anisotropy).[38] Additionally, the shear anisotropic factors A_1, A_2, and A_3 are also considered to describe the elastic anisotropy due to our investigated crystal systems including hexagonal and cubic crystal structures. A_1, A_2, and A_3 are defined as[32]

$$A_1 = \frac{4C_{44}}{C_{11}+C_{33}-2C_{13}} \quad \text{for the } \{1\,0\,0\} \text{ plane}, \quad (8)$$

$$A_2 = \frac{4C_{55}}{C_{22}+C_{33}-2C_{23}} \quad \text{for the } \{0\,1\,0\} \text{ plane}, \quad (9)$$

$$A_3 = \frac{4C_{66}}{C_{11}+C_{22}-2C_{12}} \quad \text{for the } \{0\,0\,1\} \text{ plane}. \quad (10)$$

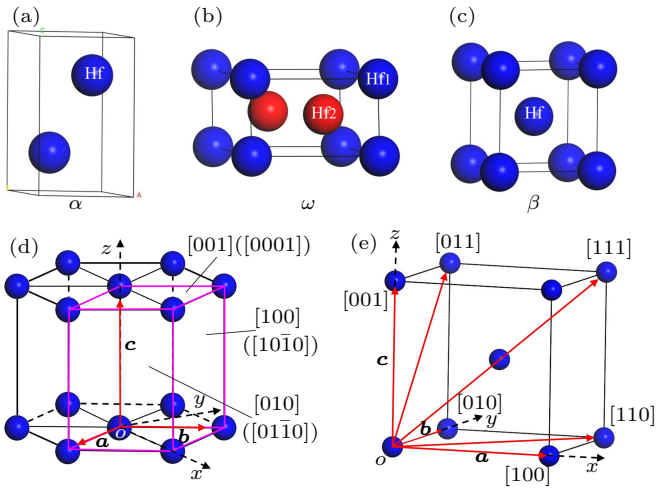


Fig. 1. Crystal structures of (a) α-Hf, (b) ω-Hf, and (c) β-Hf, as well as the indices of crystal direction and plane for (d) hexagonal and (e) cubic structures.

If $A_1 = A_2 = A_3 = 1$, the crystal is isotropic. Otherwise, it is anisotropic. For the hexagonal structure, due to $C_{11} = C_{22}$,

$C_{13} = C_{23}$, and $C_{44} = C_{55}$, A_1 equals A_2. For cubic structure, due to $C_{11} = C_{22} = C_{33}$, $C_{12} = C_{13} = C_{23}$, and $C_{44} = C_{55} = C_{66}$, $A_1 = A_2 = A_3$. These results of elastic anisotropies are listed in Table 1 for α, ω, and β phases. At 0 GPa, the calculated results of the α-Hf are consistent with that from Duan *et al.*[39] except A_3. In our calculations, $A_3 = 1$, because here the C_{66} is calculated by $C_{66} = \frac{C_{11}-C_{12}}{2}$. At ambient pressure, clearly the order of the universal elastic anisotropic index is ω-Hf $> \alpha$-Hf > 0. For compression and shear anisotropies, $A_{\text{shear}} > A_{\text{comp}} > 0$ for α and ω phases, which indicates that the shear anisotropy is larger than the compression anisotropy and the elastic moduli are dependent on different directions. In addition, for shear anisotropic factors, $A_1 = A_2 < A_3$ for α and ω phases, which also supports the conclusion that the elastic moduli are strongly dependent on different directions. Along with the increase of pressure, the data of the universal elastic anisotropic A^{U} increase monotonically for α-Hf and ω-Hf, while they decrease for β-Hf. For α-Hf, increasing the pressure from 0 to 44.8 GPa, A_{comp} and A_{shear} increase monotonically. However, A_1 and A_2 decrease, and the differences between A_1 and A_3 range from 0.194 to 0.432, which means that the dependence of the elastic moduli on different directions becomes more pronounced upon compression. Similar phenomena occur in A_{comp}, A_{shear}, A_1, A_2, and A_3 for ω-Hf within 0–73 GPa. For β-Hf, although the universal elastic anisotropic index decreases from 10.894 to 3.714 within 73.3–100 GPa, it still much larger than 0. Thus the elastic properties are still anisotropic. Although $A_{\text{comp}} = 0$ and A_{shear} decreases from 0.5214 to 0.2409 within 73.3–100 GPa, A_{shear} still does not equal 0. Similar to A^{U}, here A_1, A_2 and A_3 also decrease from 10.987 to 4.419 within 73.3–100 GPa, but they still much larger than 1. Overall, the calculated A_{shear}, A_{comp} and shear anisotropic factors (A_1, A_2, and A_3) values support this conclusion that the elastic moduli of α-Hf, ω-Hf, and β-Hf are strongly dependent on different directions. Moreover, the elastic anisotropy increases with increasing pressure for α and ω phases, while decreases upon compression for β phase.

Table 1. The calculated ratio of bulk modulus ($B_{\text{V}}/B_{\text{R}}$) and shear modulus ($G_{\text{V}}/G_{\text{R}}$), universal anisotropic index (A^{U}), percent anisotropy (A_{comp} and A_{shear}), and shear anisotropic factors (A_1, A_2, and A_2) of Hf.

Phase	Pressure (GPa)	$B_{\text{V}}/B_{\text{R}}$	$G_{\text{V}}/G_{\text{R}}$	A^{U}	A_{comp}	A_{shear}	A_1	A_2	A_3
α	0	1.002	1.009	0.047	0.0010	0.0044	0.806	0.806	1.000
	10	1.004	1.016	0.087	0.0022	0.0082	0.744	0.744	1.000
	20	1.006	1.027	0.141	0.0028	0.0133	0.684	0.684	1.000
	30	1.008	1.041	0.211	0.0040	0.0199	0.630	0.630	1.000
	40	1.012	1.048	0.254	0.0060	0.0236	0.602	0.602	1.000
	44.8	1.014	1.057	0.300	0.0069	0.0279	0.577	0.577	1.000
		1.001[a]	1.003[a]	0.016[a]	0.0016[a]	0.0003[a]	0.932[a]	0.932[a]	0.868[a]
ω	0	1.001	1.059	0.298	0.0005	0.0288	0.567	0.567	1.000
	20	1.0003	1.067	0.337	0.0001	0.0326	0.543	0.543	1.000
	40	1.0001	1.090	0.450	0.00005	0.0431	0.496	0.496	1.000
	44.8	1.0002	1.099	0.495	0.0001	0.0471	0.481	0.481	1.000
	50	1.0004	1.110	0.552	0.0002	0.0523	0.464	0.464	1.000
	60	1.0008	1.136	0.682	0.0004	0.0638	0.429	0.429	1.000
	70	1.0012	1.166	0.833	0.0006	0.0768	0.396	0.396	1.000
	73	1.0014	1.175	0.877	0.0007	0.0805	0.387	0.387	1.000
β	73.3	1.000	3.179	10.894	0	0.5214	10.987	10.987	10.987
	80	1.000	2.665	8.327	0	0.4544	8.826	8.826	8.826
	90	1.000	2.195	5.974	0	0.3740	6.832	6.832	3.832
	100	1.000	1.635	3.174	0	0.2409	4.419	4.419	4.419

[a]Ref. [39].

As a valid method to describe the elastic anisotropic behavior of a solid completely, the three-dimensional (3D) surface constructions of the directional dependence of reciprocal of Young's modulus are also investigated by the following expressions:[40]

$$\frac{1}{E} = (1-l_3^2)^2 S_{11} + l_3^4 S_{33} + l_3^2(1-l_3^2)(2S_{13}+S_{44}) \quad (11)$$

for hexagonal system,

$$\frac{1}{E} = S_{11} - 2\left(S_{11} - S_{12} - \frac{S_{44}}{2}\right)\left(l_1^2 l_2^2 + l_2^2 l_3^2 + l_1^2 l_3^2\right) \quad (12)$$

for cubic system, where S_{ij} is the usual elastic compliance constant, which is obtained from the inverse of the matrix of elastic constants; l_1, l_2, and l_3 are the direction cosines. The results of Young's modulus for α, ω, and β phases are shown in panels (a) and (c) of Figs. 2–4, as well as the corresponding shear modulus in panels (b) and (d) of Figs. 2–4. The surface in each of graphs means the magnitude of E and G in different directions. For an isotropic system, the 3D surface construction is a spherical shape. The values of anisotropy coefficient are reflected by the deviation degree from the spherical shape. In addition, we calculate Young's modulus in the three principal directions by $E_{[100]} = 1/S_{11}$, $E_{[010]} = 1/S_{22}$, and $E_{[001]} = 1/S_{33}$.

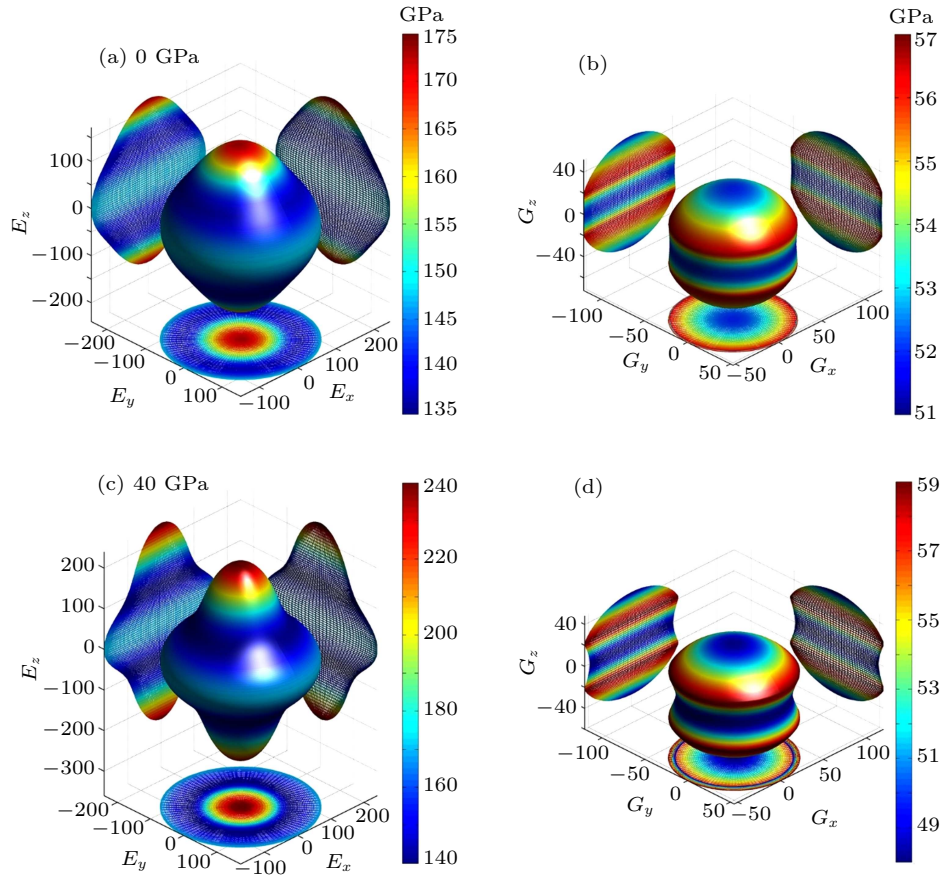


Fig. 2. Directional dependences of Young's modulus for α-Hf under (a) 0 GPa and (c) 40 GPa with the corresponding shear modulus in (b) and (d).

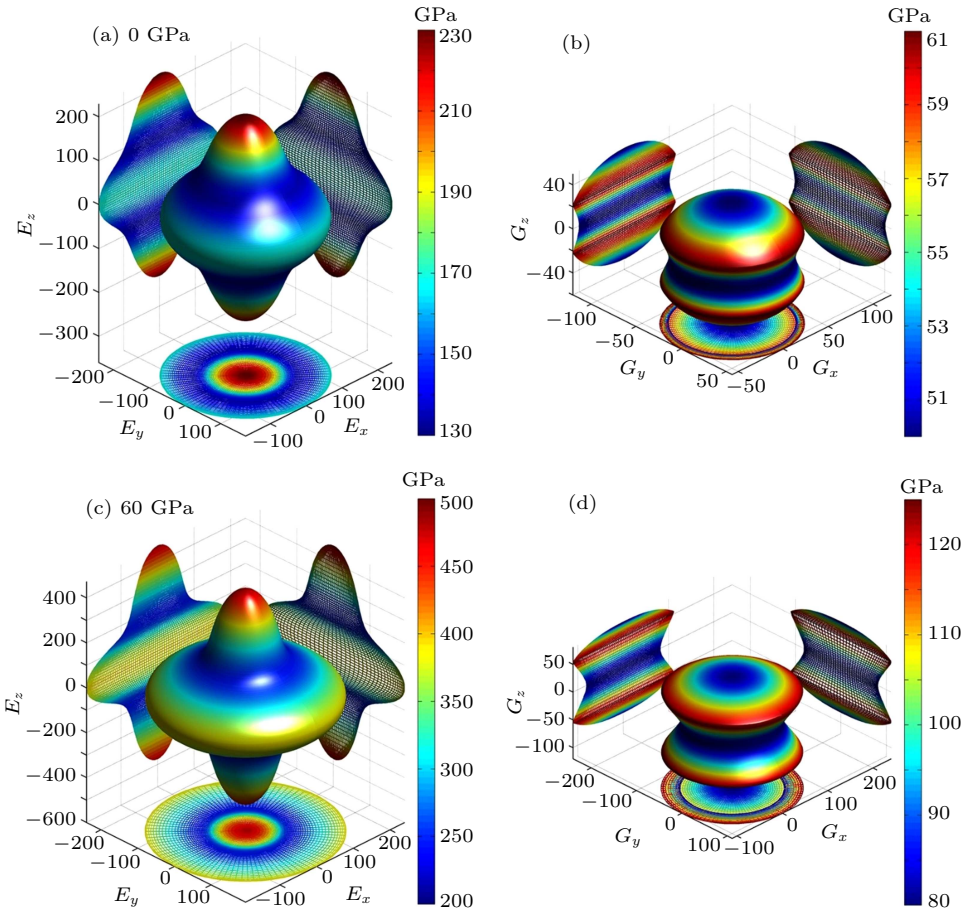


Fig. 3. Directional dependences of Young's modulus for ω-Hf under (a) 0 GPa and (c) 60 GPa with the corresponding shear modulus in (b) and (d).

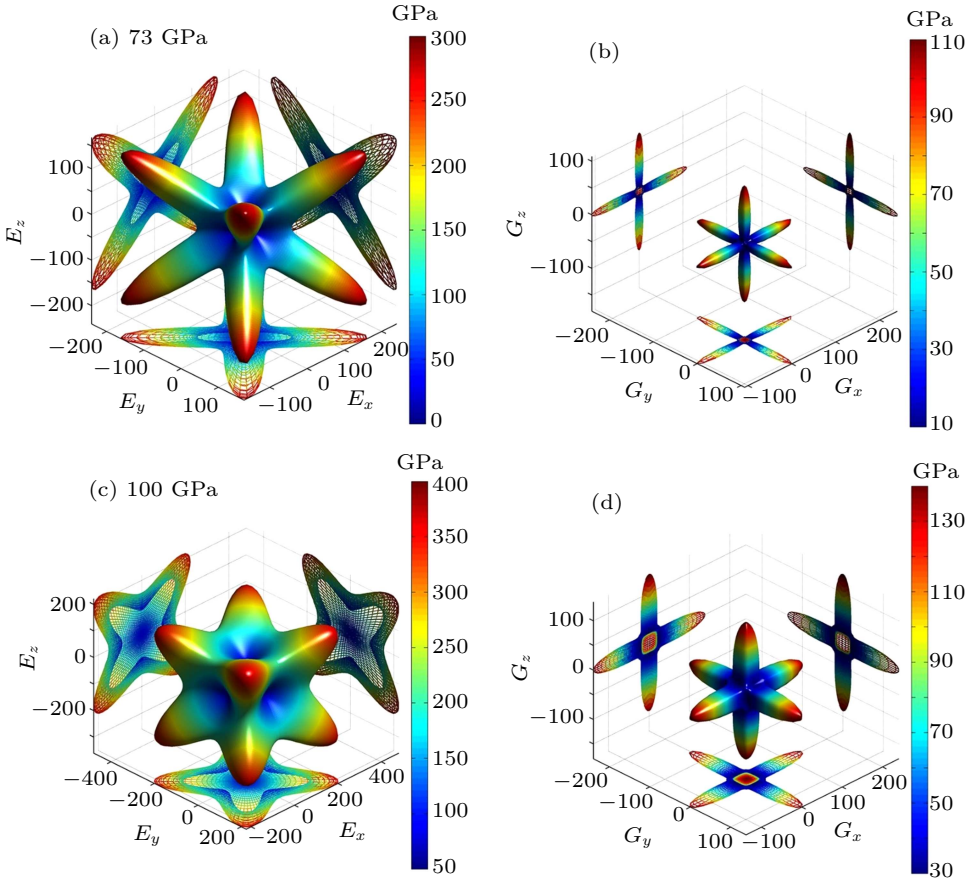


Fig. 4. Directional dependences of Young's modulus for β-Hf under (a) 73 GPa and (c) 100 GPa with the corresponding shear modulus in (b) and (d).

For the hexagonal α and ω phases, a large deviation in 3D surface constructions from the sphere indicates that Young's modulus E and shear modulus G show a strong anisotropy (see Figs. 2 and 3). Under compression, Young's modulus and shear modulus have the increasing deviation in shape from the sphere. It is suggested that Young's modulus and shear modulus show a increasing elastic anisotropy. For α phase, $E_{[100]}$ is equal to $E_{[010]} = 185.18$ GPa $< E_{[001]} = 208.33$ GPa at 0 GPa. $E_{[100]}$ is equal to $E_{[010]} = 263.16$ GPa $< E_{[001]} = 333.33$ GPa at 40 GPa. These indicate that Young's modulus along [100] or [010] direction are more compressible than along [001] direction for α-Hf. Similarly, for ω phase, $E_{[100]}$ is equal to $E_{[010]} = 163.93$ GPa $< E_{[001]} = 212.77$ GPa ($E_{[100]}$ is equal to $E_{[010]} = 294.12$ GPa $< E_{[001]} = 333.33$ GPa) at 0 (60) GPa. For β phase, Young's modulus in three principal-axial ($E_{[100]}$, $E_{[010]}$, and $E_{[001]}$) directions are 263.16 (333.33) GPa at 73 (100) GPa. Meanwhile, Young's modulus in [110] and [111] directions by using the expressions introduced in the recent report[41] are 300.75 (370.37) GPa and 500 (555.56) GPa at 73 (100) GPa. Therefore, one can conclude that Young's modulus has a strong directional dependence. The difference values in the directional Young's modulus between [111] and the principal axes direction are 199.25 GPa and 185.19 GPa for 73 GPa and 100 GPa, respectively, which indicates that Young's modulus shows an anisotropic property and the anisotropy decreases upon compression. Although the difference values are on the decrease along with the pressure increasing from 73 to 100 GPa, Young's modulus still shows a strong anisotropic property [see Figs. 4(a) and 4(c)]. As shown in Figs. 4(b) and 4(d), the largest value locates on the [100] direction while the smallest value exists on the [110] direction for shear modulus. According to these results, one can conclude that the β-Hf is much easier to stretch along the [100] direction than other directions and also easy to shear along the [110] direction. The results of 3D surface constructions also show that elastic anisotropies increase with increasing pressure for α and ω phases, while decrease upon compression for β phase. This result also supports our conclusion from the analysis of the universal elastic anisotropy indexes.

3.2. Superconductive properties

Hafnium has excellent performance for high-temperature superconductivity, especially the high-pressure β phase.[16] Now, we focus our attention on structures of the electronic, vibration modes, and the EPC in pressure range of 0–100 GPa to analyze the effect of pressure on superconductivity. The orbital-resolved band structures and the electronic DOS curves of α, ω, and β phases are plotted in Figs. 5–7.

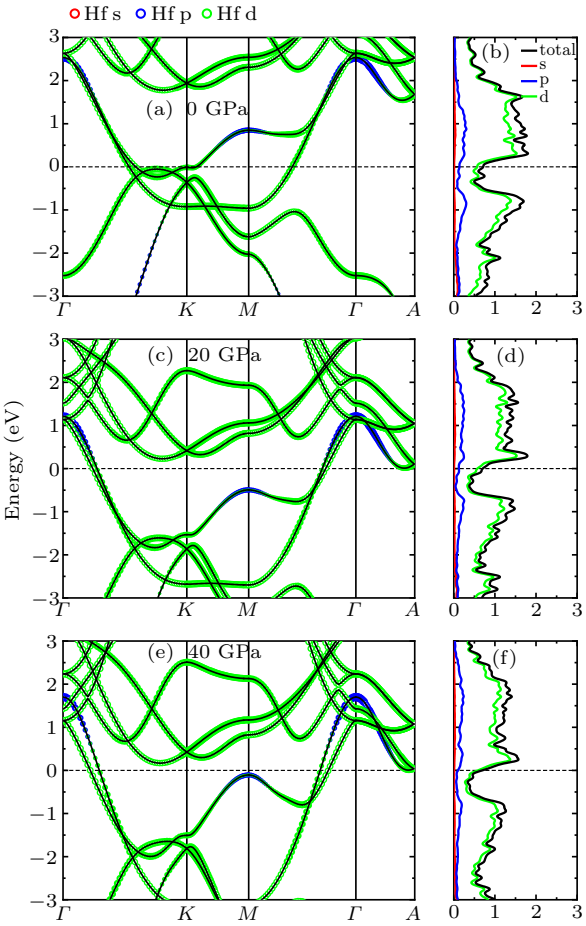


Fig. 5. Orbital-resolved band structures for α-Hf under (a) 0, (c) 20, and (e) 40 GPa, respectively, with the total and orbital-resolved local electron DOS in (b), (d), and (f).

Comparing the results at different pressures, one can see that the contribution of the bands around the Fermi energy level mainly comes from the Hf-d orbital, while the contribution from the p orbital is limited and from the s orbital is hardly seen. As the DOS curves shown in Fig. 5, for α phase, the values of total $N(E_{\rm F})$ are 0.715 states/(eV atom), 0.701 states/(eV atom), and 0.688 states/(eV atom) at 0 GPa, 20 GPa, and 40 GPa, respectively. The values of total $N(E_{\rm F})$ are decreasing with increasing pressure from 0 to 40 GPa. In addition, at 0 GPa, there is a peak (near 0.31 eV) and a valley (near -0.10 eV) lying in two sides of the Fermi energy level, respectively. Upon compressing, both of them are shifted downwards in energy level. For ω phase (see Fig. 6), there exist two different kinds of atoms: Hf1 in 1a and Hf2 in 2d sites. The $N(E_{\rm F})$ values of Hf1-d (Hf2-d) electrons are 0.500 (0.626) states/(eV atom), 0.544 (0.611) states/(eV atom), and 0.547 (0.570) states/(eV atom) at 45 GPa, 60 GPa, and 70 GPa, respectively. Along with increasing the pressure from 45 to 70 GPa, the occupied of Hf1-d electron will approach to Hf2-d electron occupation at the Fermi level. Although the d-electron occupation of Hf1 and Hf2 has an opposite evolution upon compressing around the Fermi level, the total $N(E_{\rm F})$ still increases within 45–70 GPa.

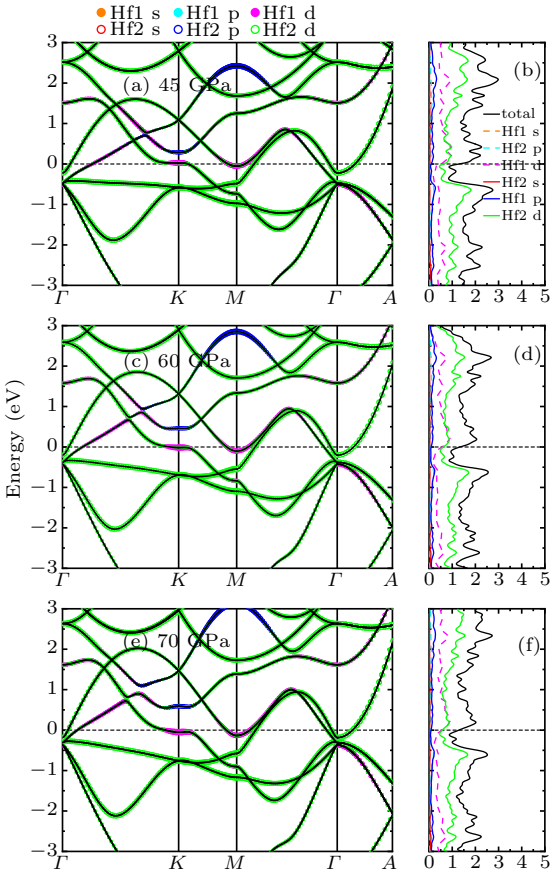


Fig. 6. Orbital-resolved band structures for ω-Hf under (a) 0, (c) 40, and (e) 60 GPa, respectively, with the total and orbital-resolved local electron DOS in (b), (d), and (f).

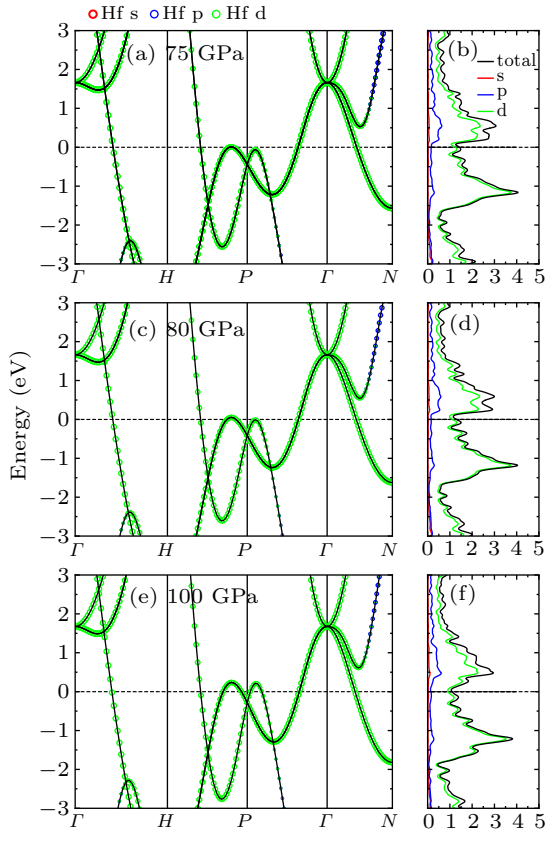


Fig. 7. Orbital-resolved band structures for β-Hf under (a) 70, (c) 80, and (e) 100 GPa, respectively, with the total and orbital-resolved local electron DOS in (b), (d), and (f).

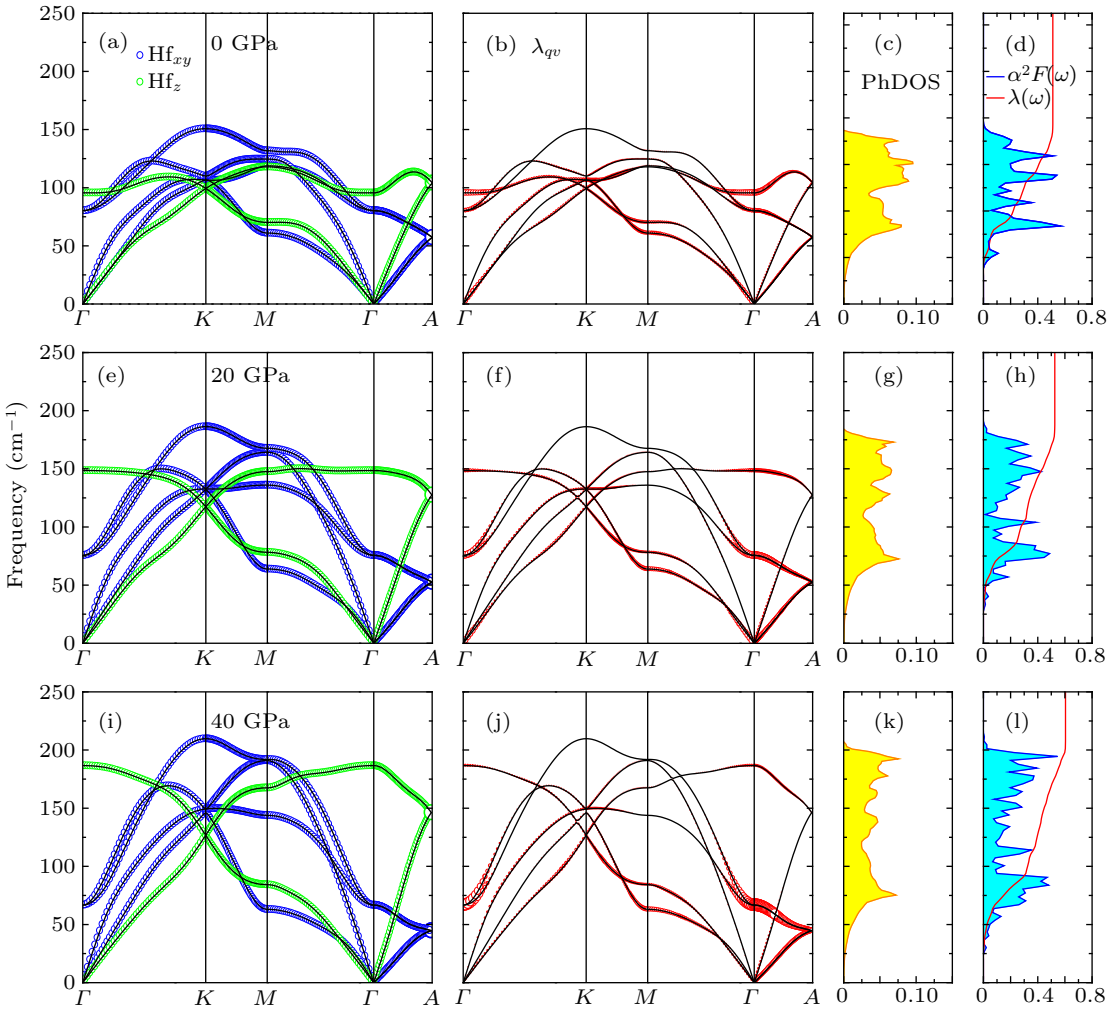


Fig. 8. Phonon dispersions, PhDOS, Eliashberg spectral function $\alpha^2F(\omega)$, and cumulative frequency-dependent of EPC $\lambda(\omega)$ for α-Hf. The phonon dispersions in (a), (e), and (i) are weighted by the motion modes of Hf atom while in (b), (f), and (j) are weighted by the magnitude of the EPC λ_{qv} ($\lambda_{qv} = \frac{\gamma_{qv}}{\pi h N(E_F)\omega_{qv}^2}$). The blue and green hollow circles in (a), (e), and (i) indicate Hf horizontal and Hf vertical modes, respectively. The magnitude of λ_{qv} is displayed with identical scale.

Moreover, there also have a peak (near 0.21 eV) and a valley (near −0.07 eV) at the conduction band and valence band, respectively, and both of them are shifted downwards in energy level upon compression. For β phase (see Fig. 7), different from the α and ω phases, although the peak and the valley also lie at nearly 0.24 eV and −0.18 eV, respectively, both of them are shifted upwards in energy level with pressure increasing. From 75 GPa to 100 GPa, the total $N(E_F)$ presents a trend of decrease from 1.436 to 1.097 states/(eV atom).

Next, we want to discuss the vibrational properties, the EPC, and the PhDOS of Hf metal, as well as the Eliashberg spectral function $\alpha^2F(\omega)$. The results are plotted in Fig. 8 for α phase at 0 GPa, 20 GPa, and 40 GPa, Fig. 9 for ω phase at 45 GPa, 60 GPa, and 70 GPa, and Fig. 10 for β phase at 75 GPa, 80 GPa, and 100 GPa, respectively. In fact, no imaginary modes are observed, which clearly indicates that α, ω and β phases are dynamically stable at given pressure domain. In addition, one can see that pressure will enhance the phonon energies. These results turn out to be the same as our recent result.[3] The phonon vibrations can be divided into two forms: in-plane vibrations Hf$_{xy}$ and out-of-plane vibrations Hf$_z$. For α and β phases, the Hf$_{xy}$ and Hf$_z$ phonon vibrations are visible in the full BZ. Different from the α and β phases, for ω phase, the in-plane vibrations (Hf1$_{xy}$ and Hf2$_{xy}$) are visible in the full BZ while the out-of-plane vibrations of the Hf1$_z$ (Hf2$_z$) occupy the frequencies region above (below) 100 cm^{-1}.

We also calculate the phonon dispersions weighted by the magnitude of the EPC λ_{qv}, the PhDOS, the Eliashberg electron-phonon spectral function $\alpha^2F(\omega)$, and the cumulative frequency-dependent of EPC $\lambda(\omega)$ and plot them in Figs. 8–10 for α, ω, and β phases, respectively. The λ_{qv}, here, according to the Migdal–Eliashberg theroy,[42] can be written as

$$\lambda_{qv} = \frac{\gamma_{qv}}{\pi h N(E_F)\omega_{qv}^2}. \tag{13}$$

The cumulative frequency dependence of EPC $\lambda(\omega)$ and the

$\alpha^2F(\omega)$ can be obtained from Eqs. (3) and (4), respectively. For α-Hf (see Fig. 8), at 0 GPa, according to our calculated $\lambda(\omega)$, one can see that the total EPC λ is equal to 0.511, and the vibrations, in the frequency below ~76 cm^{-1}, contribute 0.205 (40.1%). The phonons, in the frequency region of 76–112 cm^{-1}, contribute 0.170 (33.3%) of the total EPC, and the remaining 0.136 (26.6%) contribution comes from phonons in frequencies above 112 cm^{-1}. Increasing the pressure to 40 GPa, the total EPC λ increases to 0.605, and almost half the λ comes from the contribution of phonons in frequencies below ~93 cm^{-1}. In the frequency region 0–93 cm^{-1}, the large values of the λ_{qv} here lead to the large EPC strength, which has resulted in a peak of the PhDOS and the $\alpha^2F(\omega)$. As shown in Fig. 9, for ω phase, at 45 GPa, the total EPC $\lambda = 0.582$. In frequencies below ~65 cm^{-1}, the λ accounts for 15.3% (0.089) of the total EPC, and the large values of the EPC strength λ_{qv} here result in a peak on the $\alpha^2F(\omega)$. Most of the total λ, about 75.0%, come from the contribution of phonons in frequency region of 65–187 cm^{-1}. At 70 GPa, the total EPC λ increases to 0.727, and the phonons' contribution in frequencies below ~65 cm^{-1} increases to 21.2% (0.154) of the total EPC. However, the contribution of phonons, in the frequency region of 65–187 cm^{-1}, decreases to 59.9%. For β phase (see Fig. 10), at 75 GPa, the total EPC $\lambda = 1.624$. The phonons, in frequency region of 0–45 (45–70) cm^{-1}, contribute 30.0% (15.0%) of the total λ. Obviously, the large values of λ_{qv} along the Γ–A direction in the frequency range 0–50 cm^{-1} are mainly due to the lowest transverse-acoustics (TA1) soft mode, which results in a peak on the $\alpha^2F(\omega)$. Increasing the pressure to 100 GPa, the total EPC λ decreases to 0.941. In addition, the soft mode of the TA1 branch will gradually fade away by increasing pressure, which results in the decrease of λ. Similar results can be found in our previous work of β Zr.[43]

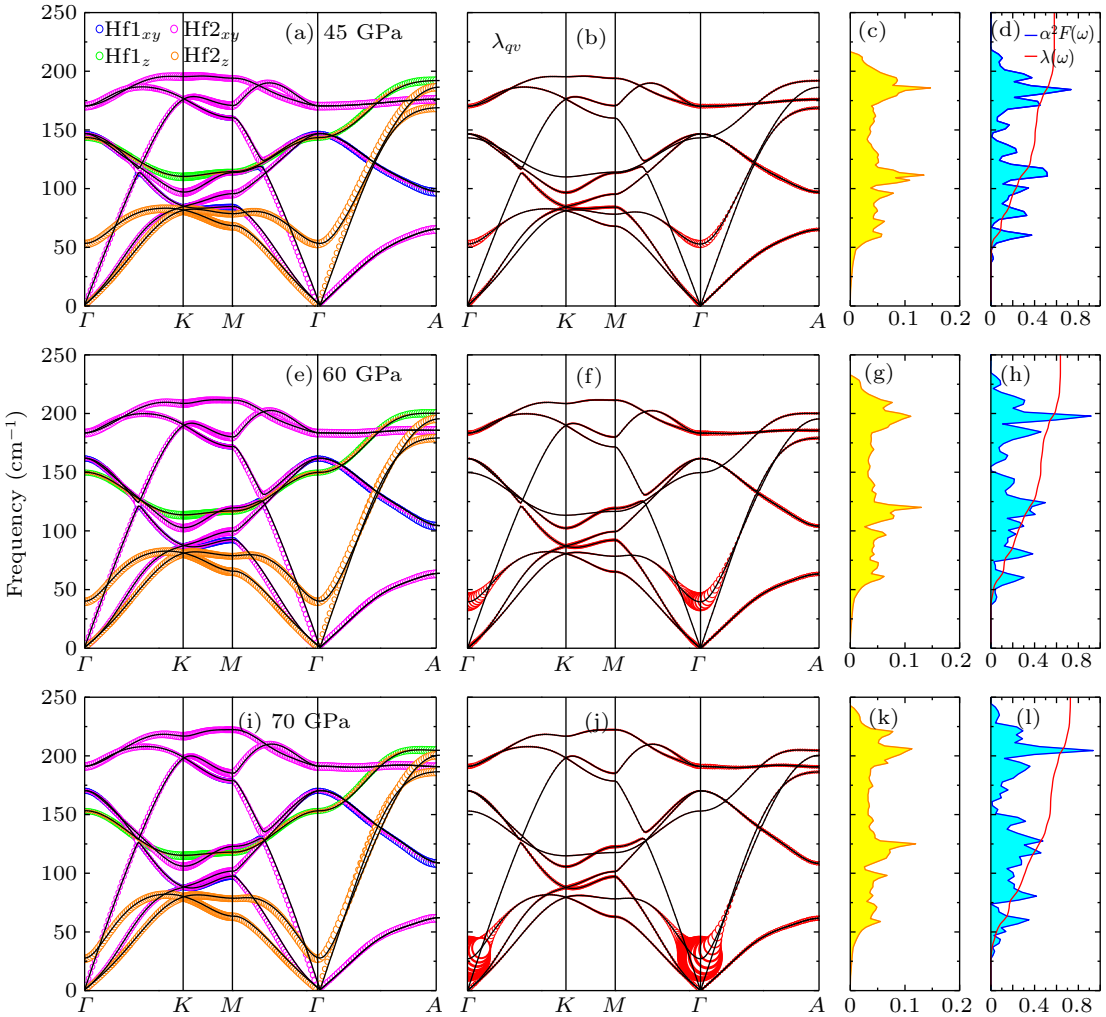


Fig. 9. Phonon dispersions, PhDOS, Eliashberg spectral function $\alpha^2F(\omega)$, and cumulative frequency-dependent of EPC $\lambda(\omega)$ for ω-Hf. The phonon dispersions in (a), (e), and (i) are weighted by the motion modes of Hf atom while in (b), (f), and (j) are weighted by the magnitude of the EPC λ_{qv} ($\lambda_{qv} = \frac{\gamma_{qv}}{\pi\hbar N(E_F)\omega_{qv}^2}$). The blue, green, magenta, and orange hollow circles in (a), (e), and (i) indicate Hf_1 horizontal, Hf_1 vertical, Hf_2 horizontal, and Hf_2 vertical modes, respectively. The magnitude of λ_{qv} is displayed with identical scale.

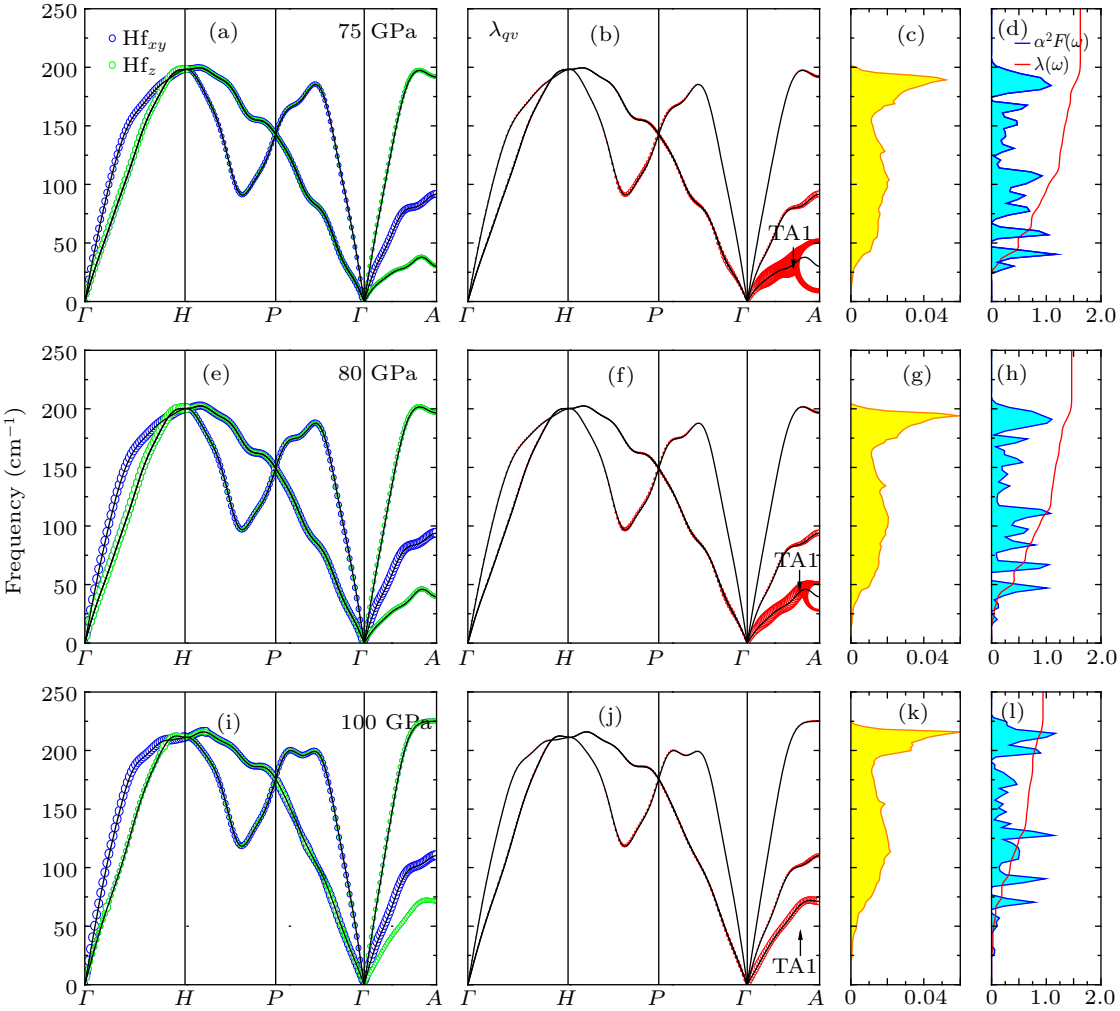


Fig. 10. Phonon dispersions, PhDOS, Eliashberg spectral function $\alpha^2F(\omega)$, and cumulative frequency-dependent of EPC $\lambda(\omega)$ for β-Hf. The phonon dispersions in (a), (e), and (i) are weighted by the motion modes of Hf atom while in (b), (f), and (j) are weighted by the magnitude of the EPC λ_{qv} ($\lambda_{qv} = \frac{\gamma_{qv}}{\pi h N(E_F)\omega_{qv}^2}$). The blue and green hollow circles in (a), (e), and (i) indicate Hf horizontal and Hf vertical modes, respectively. The magnitude of λ_{qv} is displayed with identical scale.

The superconducting transition temperatures T_c have been calculated from Eq. (1) with a typical value $\mu^* = 0.1$ is used, and plotted in Fig. 11 for these there phases. Clearly, the different phenomena are observed in the pressure dependence. The pressure coefficient of the T_c in the α and ω phases is a positive value, while the β-Hf shows a negative pressure coefficient. In addition, although our predicted values of T_c are larger than the experimental values, the pressure-dependent behaviors accord well with the experimental results.[16] According to the McMilan equation [Eq. (1)], one can see that the T_c is determined by ω_{log}, λ, and $N(E_F)$. Thus, we have calculated the ω_{log} and the λ in the pressure range 0–100 GPa and plotted them in Fig. 12. The results show that the values of the λ for α and ω phases increase with the increasing pressure, as well as the values of the ω_{log} for α phase. However, the ω_{log} change is not evident under compression for ω phase. In our previous discussion, the total $N(E_F)$ of α phase decreases with pressure. These results support this conclusion that the increase of T_c for α phase under pressure mainly originates from the increase of λ and ω_{log}, as well as the decrease of $N(E_F)$ by increasing pressure. For ω phase, although the total $N(E_F)$ of α phase increases with pressure, the $N(E_F)$ of Hf2 decreases with pressure. Moreover, Fig. 9 shows that the Hf2 phonons' vibrations contribute most of the total λ. Therefore, one can conclude that the increase of T_c for ω phase mainly originates from the increase of λ. However, for β phase, almost opposite evolutions appear on ω_{log} and λ curves in the pressure range 75–100 GPa. The increasing rate of ω_{log} is smaller than the decreasing rate of λ. Thus the decrease of T_c for β phase mainly originates from the decrease of λ in 75–100 GPa pressure domain. In addition, the lowest TA1 soft mode for β phase can lead a significant electron-phonon contribution, which has been discussed in the above paragraph. With the increasing pressure, soft vibrational mode gradually fades away. Thus, the decrease of T_c under pressure mainly originates from the fading of soft vibrational modes induced by increasing pressure. Actually, for Zr metal, similar pressure-dependent behaviors are also observed in T_c, which

has been reported in experiments by Akahama *et al.*[44] and calculations by Wang *et al.*[43] Akahama *et al.* believe that the effect of pressure on the T_c has relation with the s–d electronic transformation. For transition metals, the dT_c/dP is governed by the shape of the d-band, expressed by the quantity $dN(E_F)/dZ_d$.[45] Z_d is valence electron numbers. Compression affects the T_c in the same way as filling the d-band by adding atoms of higher valency.[44] As a same group element, the s–d transition is also a feature of Hf under pressure. Therefore, we surmise that the effect of pressure on the T_c also has relation with the s–d electronic transformation for Hf metal. Future investigations are needed to verify our speculation.

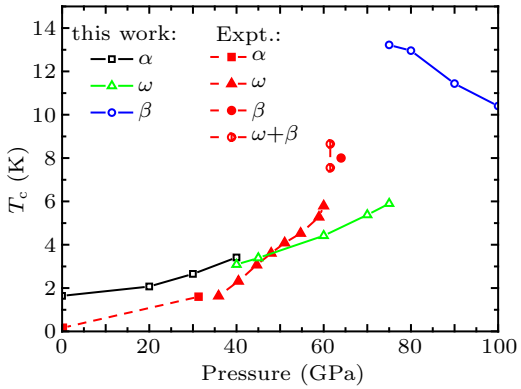


Fig. 11. Calculated superconducting transition temperature T_c versus pressure for α, ω, and β phases. The experimental values of T_c from Ref. [16] are also presented. The half right circle is an indication of a two-phase $\omega+\beta$ state of the sample under these conditions.[16]

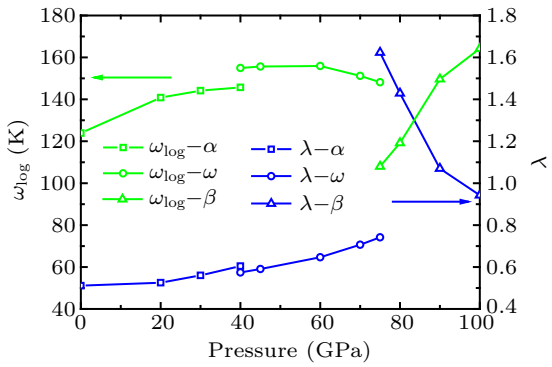


Fig. 12. Pressure dependences of logarithmic average of the vibrational frequencies ω_{log} and EPC constants λ.

4. Conclusion

In summary, the first-principles calculations are employed to investigate the elastic anisotropy and superconductive properties of hafnium metal. Hafnium is an elastic anisotropic crystal. Its elastic moduli are strongly dependent on different directions. From the anisotropic parameters and the 3D surface constructions of the E and G, one can conclude that the elastic anisotropy increases with increasing pressure for α and ω phases, while decreases under compression for β phase. In addition, our calculated T_c agrees well with experiments. Upon compression, the increase (decrease) of T_c mainly originates from the corresponding increase (decrease) behavior of the EPC constant λ.

Acknowledgment

The calculations were performed at Supercomputer Center in China Spallation Neutron Source.

Appendix A: Convergence test of electron–phonon coupling constant

It is difficult to obtain convergent λ, directly. In practical EPC matrix element calculation, the δ function can be replaced by the smearing function with a broadening width σ.[46] We are interested in the limit that $\sigma \to 0$ and the number of k points $\to \infty$. In order to obtain convergent EPC constant λ, we have extensively tested the number of k and q points for α-Hf at 0 GPa. These results are shown in Fig. A1. As shown in Fig. A1, for α-Hf at 0 GPa, with increasing the number of k or q points, the values of λ decrease. When the k and q points increase to a certain extent, the differences of λ values are small, meanwhile there is an emergence of a small separation near $\sigma = 0.02$ eV in the overlapping results. According to the results, we can say that the calculated EPC constant λ is convergent for a k-point, e.g., 24×24×16, and a q-point, e.g., 6×6×4. In addition, the corresponding σ is 0.02 eV.

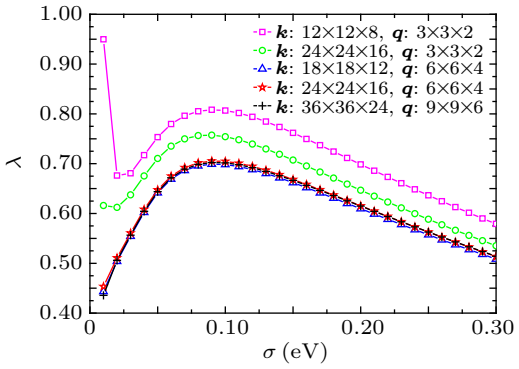


Fig. A1. Convergence test of EPC constant versus smearing parameter σ in α-Hf at 0 GPa with different k and q points.

References

[1] Wang P, Zhang N C, Jiang C L, Liu F S, Liu Z T and Liu Q J 2020 *Chin. Phys. B* **29** 076201
[2] Sun W W, Luo W, Feng Q G and Ahuja R 2017 *Phys. Rev. B* **95** 115130
[3] Zhang C B, Li W D, Zhang P and Wang B T 2019 *Comput. Mater. Sci.* **157** 121
[4] Duthie J C and Pettifor D G 1977 *Phys. Rev. Lett.* **38** 564
[5] Skriver H L 1985 *Phys. Rev. B* **31** 1909
[6] Tal A A, Katsnelson M I, Ekholm M, Jönsson H J M, Dubrovinsky L, Dubrovinskaia N and Abrikosov I A 2016 *Phys. Rev. B* **93** 205150
[7] Tonkov E Y and Ponyatovsky E G 2005 *Phase Transformation of Elements under High Pressure* (Boca Raton, FL: CRC Press)
[8] Qi X T, Wang X B, Chen T and Li B S 2016 *J. Appl. Phys.* **119** 125109
[9] Xia H, Parthasarathy G, Luo H, Vohra Y K and Ruoff A L 1990 *Phys. Rev. B* **42** 6736

[10] Hrubiak R 2012 *Exploring Thermal and Mechanical Properties of Selected Transition Elements under Extreme Conditions: Experiments at High Pressures and High Temperatures* (PhD Dissertation) (Florida International University)

[11] Pandey K K, Gyanchandani J, Somayazulu M, Dey G K, Sharma S M and Sikka S K 2014 *J. Appl. Phys.* **115** 233513

[12] Chen Q and Sundman B 2001 *Acta Mater.* **49** 947

[13] Novoselov D, Anisimov V I and Ponosov Y S 2018 *Phys. Rev. B* **97** 184108

[14] Ostanin S A and Trubitsin V Y 2000 *Comput. Mater. Sci.* **17** 174

[15] Ahuja R, Wills J M, Johansson B and Eriksson O 1993 *Phys. Rev. B* **48** 16269

[16] Bashkin I O, Nefedova M V, Tissen V G and Ponyatovsky E G 2004 *JETP Lett.* **80** 655

[17] Gyanchandani J S, Gupta S C, Sikka S K and Chidambaram R 1990 *J. Phys.: Condens. Matter* **2** 6457

[18] Ming L, Manghnani M H and Katahara K W 1981 *J. Appl. Phys.* **52** 1332

[19] Tittman B, Hamilton D and Jayaraman A 1964 *J. Appl. Phys.* **35** 732

[20] Degtyareva V F, Karimov Yu S and Rabinkin A G 1974 *Sov. Phys.-Solid State (Engl. Transl.)* **15** 3436

[21] Bashkin I O, Tissen V G, Nefedova M.V and Ponyatovsky E G 2007 *Physica C* **453** 12

[22] Heiniger F, Bucher E and Muller J 1966 *Physik der kondensierten Materie* **5** 243

[23] Hamlin J J 2015 *Physica C* **514** 59

[24] Perdew J P and Wang Y 1992 *Phys. Rev. B* **45** 13244

[25] Perdew J P, Burke K and Ernzerhof M 1996 *Phys. Rev. Lett.* **77** 3865

[26] Giannozzi P, Baroni S and Bonini N et al. 2009 *J. Phys.: Condens. Matter* **21** 395502

[27] Baroni S. Gironcoli De S, Dal Corso A and Giannozzi P 2001 *Rev. Mod. Phys.* **73** 515

[28] Allen P B and Dynes R C 1975 *Phys. Rev. B* **12** 905

[29] McMillan W L 1968 *Phys. Rev.* **167** 331

[30] Ranganathan S I and Ostoja-Starzewski M 2008 *Phys. Rev. Lett.* **101** 055504

[31] Chung D H, Buessem W R, Vahldiek F W and Mersol S A 1968 *Anisotropy in Single Crystal Refractory Compounds* (New York: Plenum Press)

[32] Ravindran P, Fast L, Korzhavyi P A, Johansson B, Wills J and Eriksson O 1998 *J. Appl. Phys.* **84** 4891

[33] Voigt W 1928 *Lehrburch der Kristallphysik* (Leipzig: Teubner)

[34] Reuss A 1929 *J. Appl. Math. Mech.* **9** 49

[35] Hill R 1952 *Proc. Phys. Soc. A* **65** 349

[36] Watt J P and Peselnick L 1980 *J. Appl. Phys.* **51** 1525

[37] Haines J, Leger J M and Bocquillon G 2001 *Annu. Rev. Mater. Res.* **31** 1

[38] Ozisik H B, Colakoglu K and Deligoz E 2012 *Comput. Mater. Sci.* **51** 83

[39] Duan Y H, Wu Z Y, Huang B and Chen S 2015 *Comput. Mater. Sci.* **110** 10

[40] Nye J F 1985 *Physical Properties of Crystal: Their Represent by Tensors and Matrices* (New York: Oxford University Press)

[41] Sun L, Gao Y M, Xiao B, Li Y F and Wang G L 2013 *J. Alloys Compd.* **579** 457

[42] Giustino F 2017 *Rev. Mod. Phys.* **89** 015003

[43] Wang B T, Zhang P, Liu H Y, Li W D and Zhang P 2011 *J. Appl. Phys.* **109** 063514

[44] Akahama Y, Kobayashi M and Kawamura H 1990 *J. Phys. Soc. Jpn.* **59** 3843

[45] Eichler A and Cey W 1972 *Z. Physik* **251** 321

[46] Gao M, Li Q Z, Yan X W and Wang J 2017 *Phys. Rev. B* **95** 024505